Journal Pre-proof

Study of the evolution of drying-induced flow properties for pulverised cassava grits

Hamed J. Sarnavi, Marcelo Precoppe, Hamid Salehi, Michael S.A. Bradley, Pablo García-Triñanes

PII: S0260-8774(22)00275-8

DOI: https://doi.org/10.1016/j.jfoodeng.2022.111221

Reference: JFOE 111221

To appear in: *Journal of Food Engineering*

Received Date: 8 April 2022

Revised Date: 29 June 2022

Accepted Date: 21 July 2022

Please cite this article as: Sarnavi, H.J., Precoppe, M., Salehi, H., Bradley, M.S.A., García-Triñanes, P., Study of the evolution of drying-induced flow properties for pulverised cassava grits, *Journal of Food Engineering* (2022), doi: https://doi.org/10.1016/j.jfoodeng.2022.111221.

Credit Author Statement

Hamed J. Sarnavi: Writing Original Draft, Conceptualization, Investigation, Software, Formal analysis, Visualization. **Marcelo Precoppe:** Supervision, Project administration, Funding acquisition, Resources, Writing - Review & Editing. **Hamid Salehi:** Conceptualization, Investigation, Writing - Review & Editing. **Michael S.A. Bradley:** Supervision, Resources, Methodology, Conceptualization, Investigation. **Pablo García-Triñanes:** Conceptualization, Methodology, Formal analysis, Writing - Review & Editing, Supervision, Project administration.

Study of the evolution of drying-induced flow properties for pulverised cassava grits

Hamed J.Sarnavi [a*], Marcelo Precoppe [a], Hamid Salehi [b, c], Michael S.A.Bradley [c], Pablo García-Triñanes [b,c]

a) Natural Resources Institute, Faculty of Engineering & Science, University of Greenwich, Central Avenue, Chatham Maritime, Kent ME4 4TB, UK
b) Materials and Chemical Engineering Group, School of Engineering, University of Greenwich, Central Avenue, Chatham Maritime, Kent ME4 4TB, UK
c) Wolfson Centre for Bulk Solids Handling Technology, Faculty of Engineering & Science, University of Greenwich, Central Avenue, Chatham Maritime, Kent ME4 4TB, UK

* Corresponding author email: h.j.sarnavi@gre.ac.uk

Nomenclature

PFT	Powder Flow Tester
SEM	Scanning Electron Microscopy
LDA	Laser Diffraction Analysis
PSD	Particle Size Distribution
SSA	Specific Surface area
RAS	Rotary Abrasive Surface
RCB	Rotary Cutting Blade
ffc	Flow Function
τ	Shear stress (kPa)
σ	Normal stress (kPa)
$\sigma_{cons.}$	Normal consolidation stress (kPa)
(σ_f, τ_f)	Failure point
$(\hat{\sigma}_{psh}, \hat{\tau}_{psh})$	Pre-shear steady state failure point
C	Cohesion strength (kPa)
T	Tensile strength (kPa)
n	Shear index in Warren-spring model (Dimensionless)
φ_e	Effective angle of internal friction (Degree)
φ_{sf}	Internal friction at steady-state flow (Degree)
$\Delta\varphi_{e-sf}$	Relative difference between effective and steady-state angles of internal friction (%)
σ_c	Unconfined yield strength (kPa)
σ_1	Major principal consolidation normal stress (kPa)
σ_{f1}	Normal stress at the failure plane of unconfined uniaxial compression test (kPa)
σ_{f2}	Normal stress at the endpoint of yield locus (kPa)
r	Consolidation's Mohr's circle Radius of the consolidation stress (kPa)
ρ_b	Bulk density (kg/m^3)
ρ_0	Bulk density without consolidation history (kg/m^3)
a	an indicator of the exponential dependency of bulk density on consolidation stress

Abstract

Determining the bulk flow properties of pulverised cassava grits is in high demand as designing efficient handling and drying systems remains a bottleneck step in the cassava value chain. A shear tester was used to collect the shear-to-failure data for samples taken at three drying stages. The flow properties were estimated based on the nonlinear Warren-Spring yield loci. The cassava grits' morphology and particle size distribution were also examined by scanning electron microscopy, mechanical sieving, and laser diffraction analysis. Drying reduced the cohesion and tensile strength, respectively, from 1.88 and 0.87 kPa to 0.16 and 0.12 kPa under 4.8 kPa of consolidation normal stress. Based on the flow function index (1/*ffc*), the very cohesive ($0.66<1/ffc<0.86$) wet sample with 46 % wet-based moisture content evolved to cohesive ($0.29<1/ffc<0.43$) at 31 % of moisture content. It eventually approached a free-flowing ($0.07<1/ffc<0.15$) state towards the end of the drying process at 14 % moisture content.

Keywords: Cassava; Flow properties; Warren-Spring; Tensile strength; Cohesion; Internal friction

Cohesion and tensile strength increase with moisture content up to 1.8 kPa and 0.87 kPa, respectively.

1 Introduction

Cassava (*Manihot esculenta* Crantz) has recently captured the attention of the global food business due to its unique characteristics that include highly valued nutritional benefits. According to FAO (2021), as of 2020, world cassava production accounted for 302 million tonnes; Africa's total production stood at about 193 million tonnes (about 64% of world production) (FAO, 2021). It has been speculated that the broader utilisation of cassava products can be a catalyst for rural industrial development and raise the incomes of farmers, processors, and traders. It can also contribute to the food security status of its producing and consuming households (Plucknett et al., 2000). However, there is a major constrain for the development of cassava for farmers, processors, and consumers alike, due to large distances between farms and markets (Beeching, 2001), as this crop suffers from a rapid postharvest physiological deterioration, typically 24-48 hours (Westby, 2002). However, its postharvest processing is not yet fully developed on an industrial scale and is processed mainly at small-scale processing centres across Africa (Westby, 2002). As a result of cassava's perishable nature, the drying operation takes precedence over other preservation techniques, where the wet product with an average moisture content of 50 % wb is turned into a dried product of about 14 % wb. (Balagopalan, 2002). It is a common practice to turn the peeled roots into a mash by using fast-rotating cutting edges or abrasive surfaces, followed by the mechanical dewatering and a subsequent pulverising step.

Attaining the optimum handling and processing condition relays heavily on having a deep knowledge of the behaviour of the bulk particulate product during storage, handling, and processing (Fitzpatrick et al., 2004). Bulk density, cohesion, tensile strength, internal friction, and the derived flow functions are important bulk properties representing the flow behaviour of a product. However, very little information is available in the literature regarding the relationship between cassava products' physical and flow properties, although flow properties of similar food materials have been characterised and reported. Teunou & Fitzpatrick (1999, 2000) studied the flow properties of flour, tea and whey permeate using an annular shear cell (Teunou & Fitzpatrick , 1999) in a chamber with controlled relative humidity and temperature and a Jenike shear cell (Teunou & Fitzpatrick , 2000). Later, Fitzpatrick (2004) implemented a Jenike shear cell to study different food products such as tea, sugar, corn starch, salt, cellulose, maltodextrin, cocoa, wheat flour, non-fat milk and determined yellow corn flour (Fitzpatrick, 2004). Sun (2016) also used a ring shear tester (RST-XS, Dietmar Schulze, Wolfenbüttel, Germany) to determine the flow properties of microcrystalline cellulose powder over a low range of moisture content between 1.6-10.9 % (Sun, 2016).

Flowability is generally determined based on synergistically interacting factors, including particle morphology and size distribution, chemical composition, environmental conditions and consolidation stress (Schulze, 2008; Teunou & Fitzpatrick, 1999, 2000). Larger particles tend to promote the flowability of bulk solids due to presenting a lower contact area between particles (Teunou et al., 1999). The flow behaviour of bulk solids is also directly influenced by the morphology and shape of the particles. Due to the interlocking between particles, their resistance to flow would mitigate with smoother particles. In comparison, irregular sharp-edge shapes intensify the interlocking phenomena and worsen the flowability (Amagliani et al., 2016). For a given bulk solid, the flowability also depends on the interparticle interactions, which is a function of their physical and chemical composition. For example, the fat tends to increase cohesiveness (Fitzpatrick et al., 2004), protein-enriched ingredients typically show easy-flowing behaviour (Amagliani et al., 2016), and glycerol concentration promotes the compressive strength of starchy cassava granules (Fadeyibi et al., 2014). Sun (2016) has mentioned that the particle's surface modifications by moisture caused a deterioration in the powder flow properties of the microcrystalline cellulose when exposed to different levels of relative humidity (Sun, 2016). Even though several studies have reported the bulk flow properties' dependency on the moisture content (Fitzpatrick et al., 2004; Landillon et al., 2008; Opaliński et al., 2012; Opaliński et al., 2016; Sun, 2016; Juarez-Enriquez et al., 2017; Romuli et al., 2017; Jung et al., 2018; Juarez-Enriquez et al., 2019; Salehi et al., 2021); the relevant works devoted to cassava and, in particular to pulverised grits, are scarce. However, Romuli et al. (2017) studied the impact of drying on the characteristics of cassava grits, including bulk density, angle of repose, and sliding friction, with an emphasis on the effect of particle size distribution. Their findings showed no apparent difference between wet and dried cassava grits for their angles of repose and sliding frictions.

Although moisture content is one of the most critical parameters for the flow properties of food powders, systematic information on the variation of the flow properties during drying is lacking. It is crucial to know how cassava grits' flow characteristics change as their moisture content changes during the drying process. That is to say, the flow characteristics of pulverised cassava grits influence the trouble-free design of handling and feeding systems.

This study investigates the flow behaviour of pulverised cassava grits prepared using Rotary Cutting Blades (RCB) or Rotary Abrasive Surface (RAS). The main objective is to determine the flow properties at different stages of drying as wet (46% wb.), partially dried (31% wb.), and dried (14% wb.). A Powder Flow Tester (PFT), developed at The Wolfson Centre in collaboration with Brookfield Engineering and a few food manufacturer partners (R. Berry et al., 2015), was used to measure both incipient and steady-state failure points under different consolidation conditions. Further theoretical analysis of the measured data was adopted using the nonlinear yield model of Warren-Spring. The physical properties of the samples were characterised using Scanning Electron Microscopy (SEM) imaging, mechanical sieving, and laser diffraction analysis (LDA).

2 Material and Methods

2.1 Sample preparation

Waxed cassava roots were purchased from a local market. Two ways were selected to turn the peeled roots into the cassava mash. First, a kitchen food blender (Moulinex LM2211) was used to represent the cassava grits prepared with RCB. Each batch containing 250 g of chopped roots was blended for 5 minutes. Subsequently, an electrical cheese grater (Sirman GP) was used to represent the cassava grits prepared with RAS. The resulting mash was dewatered mechanically for 10 minutes under 20 kPa pressure in muslin bags of 0.3 m × 0.2 m, separately for RCB and RAS samples of cassava grits. Obtained cassava cakes were pulverised and turned into bulk cassava grits. The grater tool previously stated was used to pulverise the cake bits. Figure 1 depicts the sequential preparation stages followed for different cassava grit samples.

Averaged moisture content values along with the corresponding standard deviations were measured in triplicate using a moisture analyser (MB120, Ohaus, NJ, USA), set to fast drying with a maximum temperature of 60 ℃, as 46±1.2 % wb and 47±1.0 % wb, respectively for RCB and RAS samples of cassava grits. Afterwards, a laboratory convection drying rig, GUNT CE130, Germany, shown in Figure 1, was used to reduce the moisture content of the samples into two levels of 31 % wb and 14 % wb. The partially dried samples had 31±1.1 % wb and 30±1.60 % wb, whereas the dried samples had 13±1.2 % wb and 14±0.6 % wb, respectively for RCB and RAS. The fresh pulverised cassava grits were gently spread over three trays, and the excess grits were scraped off using a ruler. Hot air passed over three stainless-steel trays of 340 mm * 310 mm, each holding around 300 g of wet sample. Data acquisition was performed using the equipment's software twice a second. A delicate frame had the trays weighed on a scale with 0.1 g precision. Drying was conducted by forcing 670 m^3/h of hot air flow at 70 ℃ with 12 % relative humidity for an adequate time. The heat transfer mechanism was convection, giving results comparable to common methods practised in Africa, described elsewhere (Precoppe et al., 2020). Every set of experiments was completed on the same day with fresh samples to eliminate any unnecessary errors from the storage or preservation conditions.

2.2 Particle size and morphology

Morphological characterisation of dried samples was conducted using SEM images (TM3030 Plus Benchtop Electron Microscope Hitachi, Japan). The dried samples were spread thinly on carbon tape, one layer of powder was applied to the stubs, and the samples were sputter-coated with gold to make them conductive before analysis, using an Edwards S150B sputtering equipment. After coating, the samples were scanned under a vacuum to capture the microstructural images. The acceleration voltage used was 1 kV. Images were acquired at different magnifications ranging between ×30 and ×5000.

Mechanical sieving and LDA were employed to characterise particle size in samples ranging from small particles to coarse agglomerates and fibrous flecks. According to ISO-3310-1 (2016), a stack of sieves with aperture sizes 3150, 2000, 1000, 630, 425, 250, and 100 µm was agitated in an Octagon-200 test sieve shaker for 5 min at 3 mm of amplitude. The approach was only used for samples that had been completely dried (14 % wb.) because the early efforts indicated substantial agglomeration during sieving samples with higher moisture content. The net weights of retained grits on each sieve were measured using a digital balance Sartorius LA8200S (AG, Germany) and then divided by the total weight of 250 g to give a percentage retained in each sieve.

Volume-weighted particle size analysis was conducted as described in (Lanzerstorfer, 2020). A Sympatec HELOS/RODOS (Clausthal-Zellerfeld, Germany) Laser Diffraction particle size analyser equipped with an R5 lens (measuring range: 0.5/4.5–875 µm) was used for aerosolised samples. D_{10}, D_{50}, and D_{90} were described as particle sizes below which 10 %, 50 %, and 90 % of the sample volume are found, respectively. Span values were also obtained to determine the distribution width using Eq. 1.

$$Span = \frac{D_{90} - D_{10}}{D_{50}} \quad \text{Eq. 1}$$

Furthermore, the specific surface area (SSA) was calculated by dividing the total area of the particles by the total weight.

2.3 Flowability tests

Flow properties and bulk density of wet, partially dried, and dried samples for RCB and RAS grits were determined with a shear tester of PFT, Brookfield AMETEK, as described in (R. Berry et al., 2015; R. J. Berry & Bradley, 2007). The values of 1.0 mm/s and 1 rev/h were set to the axial and torsional lid's speeds, respectively. The 6-inch 304 stainless steel vane lid and the 230 mL aluminium sample trough were used. Table 1 shows four selected levels of normal stress consolidation geometrically spaced across the whole range of the PFT normal consolidation stress, from 0.482 kPa to 4.819 kPa, as well as their corresponding over-consolidated failure stresses.

Figure 2 shows schematic illustrations of shear-to-failure points at a certain consolidation stress level used to determine the flow properties. The failure envelopes were considered to define an area in $\sigma - \tau$ plane that delineates stable and unstable stress states for a given consolidation load.

Even though the repeatability of the measured failure points can be secured by using PFT (R. J. Berry & Bradley, 2007), the critical role of the analysis procedure in expressing the yield loci is still a challenging subject (Ashton et al., 1965; Hirota et al., 2007; García-Triñanes et al., 2019). The criticality comes when it must secure the back extrapolation towards the zero consolidation stress states to predict cohesion and tensile strength (García-Triñanes et al., 2019). Previous studies on cohesive materials' behaviour in shearing (R. J. Berry & Bradley, 2007; Hirota et al., 2007; Schulze, 2008; R. Berry et al., 2015) recognise a convex upward curvature in the lower consolidation stress. Therefore, the Warren-Spring model, Eq. 2, was used. This model is broadly described in the literature and offers a better means to estimate the cohesion and tensile strength as an alternative to the arduous experimental methods needed, specifically for cohesive materials (Ashton et al., 1965; Hirota et al., 2007; García-Triñanes et al., 2019).

$$\frac{\tau}{C} = \left[\frac{\sigma}{\sigma_T} + 1\right]^{\frac{1}{n}} \qquad \text{Eq. 2}$$

Where C is cohesion, σ_T is the tensile strength, and n is the curvature number or shear index. Assigning a unit value to the parameter n will remove the curvature and represent the Mohr-Coulomb model. The linear model is implemented more frequently when dealing with free-flowing materials.

Theoretically, the premises of the analysis procedure are based on finding the best possible combination of the three parameters: σ_T, C, and n. After conducting the fitting task, other flow properties of cassava samples, such as major principal consolidation normal stress (σ_1), unconfined yield strength (σ_c), internal friction as effective (φ_e) and steady-state flow (φ_{sf}) angles, as depicted in Figure 2, using Mohr's circle analysis as follows.

It is important to note that the Warren-Spring model was applied using the previously accepted guidelines in PFT software for selecting the cut-off points for creating the linear Mohr-Coulomb failure yield loci, as mentioned in (R. J. Berry & Bradley, 2007). The geometrical characteristics of two Mohr's circles, which determine the other flow properties shown in Figure 2-a, were discovered by solving two sets of nonlinear equations. The first set, Eq. 3 and Eq. 4, characterised a Mohr circle (coloured blue in Figure 2-a) passing through the origin and touching the yield locus. It resulted σ_{f1} and σ_c, where the former one represents the failure point in an analogous unconfined compression test.

Condition of contacting yield locus

$$\left(C\left[\frac{\sigma_{f1}}{\sigma_{\mathrm{T}}}+1\right]^{\frac{1}{n}}-0\right)^2+\left(\sigma_{f1}-\frac{\sigma_c}{2}\right)^2=\left(\frac{\sigma_c}{2}\right)^2 \qquad \text{Eq. 3}$$

Condition of tangency

$$\frac{C^2}{{\sigma_{\mathrm{T}}}^2 n^2}\left[\frac{\sigma_{f1}}{\sigma_{\mathrm{T}}}+1\right]^{\frac{2-2n}{n}}=\frac{\left(\frac{\sigma_c}{2}-\sigma_{f1}\right)^2}{\sigma_{f1}\sigma_c-{\sigma_{f1}}^2} \qquad \text{Eq. 4}$$

The larger Mohr circle, shown as red in Figure 2-a, was determined by simultaneously solving Eq. 5, Eq. 6, and Eq. 7. It passed through recorded steady-state failure points of $(\hat{\sigma}_{psh}, \hat{\tau}_{psh})$ and touched the previously obtained Warren-Spring failure yield locus at the endpoint of this locus (σ_{f2}, τ_{f2}).

Condition of passing through pre-shear point	$\hat{\tau}_{psh}{}^2 + \left(\hat{\sigma}_{psh} - (\sigma_1 - r)\right)^2 = r^2$	Eq. 5
Condition of contacting yield locus	$(C\left[\frac{\sigma_{f2}}{\sigma_\mathrm{T}} + 1\right]^{\frac{1}{n}} - 0)^2 + \left(\sigma_{f2} - (\sigma_1 - r)\right)^2 = r^2$	Eq. 6
Condition of tangency	$\frac{C}{n\sigma_\mathrm{T}}\left[\frac{\sigma_{f2}}{\sigma_\mathrm{T}} + 1\right]^{\frac{1-n}{n}} = \frac{\sigma_1 - \sigma_{f2} - r}{\sqrt{r^2 - \left(\sigma_{f2} - (\sigma_1 - r)\right)^2}} = \frac{\sigma_1 - \sigma_{f2} - r}{C\left[\frac{\sigma_{f2}}{\sigma_\mathrm{T}} + 1\right]^{\frac{1}{n}}}$	Eq. 7

Where, r is the circle's radius representing the steady-state yield limit. An envelope was then built for each sample holding a specific moisture content and having a given normal stress history by adding parts. The first part denoting the incipient failure points was formed by the regressed Warren-Spring model of Eq.2 over the normal stress range of $(-\sigma_\mathrm{T}, \sigma_{f2})$. The second part was attributed to the pre-shear failure points expressed by a section of the consolidation Mohr circle laid over the normal stress range of (σ_{f2}, σ_1). σ_{f2} determined the transition between these two different states of failure. However, this transition can also be expressed by the angles of internal friction, as seen in Figure 2-b. Hence, the internal friction was also characterised by the effective angle of internal friction (φ_e), and the angle of internal friction at steady-state flow (φ_{sf}), as shown in Figure 2-b, using Eq. 8 and Eq. 9, respectively.

$$\sin\varphi_e = \frac{\sigma_1 - \sigma_2}{\sigma_1 + \sigma_2} \qquad \text{Eq. 8}$$

$$\tan\varphi_{sf} = \frac{\hat{\tau}_{psh}}{\hat{\sigma}_{psh}} \qquad \text{Eq. 9}$$

2.4 Statistical Analysis

Particle size characterisation and shear tests were carried out in triplicate, and the results were presented as mean values and standard deviation values. The statistical and mathematical calculations were coded in Python using Scipy library (Virtanen, et al, 2020). Visualisation of results is handled by the Matplotlib library (Hunter, 2007). Analysis of variance was carried out at a significance level of $P<0.05$. Fitting the shear-to-failure data over the Warren-Spring equation (Eq.2) and solving Eq.3 to Eq.7 were carried out by the least-squares method with the convergence criterion of 10^{-6} using "scipy. optimise" library.

3 Results and Discussion

3.1 Particle morphology and size

The failure strength of bulk solids is significantly influenced by the morphology and size distribution of the constitutional components. Figure 3 depicts the shape of cassava particles using a scanning electron microscope at various magnification levels. No apparent differences in the morphology of the grits' entities with regard to their production method were seen at the observed magnification levels. The observed granules at ×5000 and ×1000 magnification levels can be described as truncated round ovals, sometimes appearing as irregular polygonal particles. These granules are made up of two distinct glucose polymers - amylopectin and amylose (Han et al., 2019), owning smooth surfaces with no cracks. According to (Dudu et al., 2019), they form approx. 85% of the cassava samples, where protein (1.55%), lipids (0.84%), crude fibre (1.73%), and 1.64% ash form the rest. Truncated surfaces can impact the bulk properties of cohesion and tensile strength, resulting in inferior flowability by enhancing van der Waals forces and mechanical interlocking between granules.

Furthermore, due to the limitations of SEM imaging of wet samples, the presence of water can be dominant either by inflating the granules or by sculpting inter-particle bridges and enhancing capillary forces (Salehi et al., 2021). At ×100 magnification level, the clusters of starch granules can be seen along with individual particles. The acquired SEM images also show various irregular shapes of clusters. At a magnification level of ×30, the effects of applying various preparation techniques were palpable. Qualitative observation of the variance in cluster sizes was carried out through further PSD analyses. Figure 4 depicts the results of the particle size characterisations conducted according to volumetric and weight measurements by LDA (Figure 4-a) and sieving (Figure 4-b), respectively.

The population of individual granules is expected to increase by reducing the moisture content, as evidenced by Figure 4. Based on the size distribution measurements, it can be postulated that the preparation methods, RCB or RAS, caused different shapes and sizes of the clusters formed by individual particles agglomerated. The span values in Figure 4 agreed with the SEM images at ×5000 magnification, showing a range of variation in the shape and size of starch granules, between 5-18 μm. This finding also agrees with the work (Airlangga et al., 2020; Zhang et al., 2018). According to weight-based measurements of sieving, dried RCB grits showed a wider span of 2.44 with D50 equal to 225 μm compared to RAS grits with a D50 of 385 μm and a span of 1.56.

3.2 Bulk density

Bulk density, ρ_b, was used to characterise the bulk structure of samples in collaboration with their PSD and moisture content. Figure 5 plots the measured bulk density values for wet, partially dried, and dried samples subjected to several consolidation stresses.

The analysis of variance at a 95% confidence level showed that the preparation procedure did not affect the variation of ρ_b with increasing consolidation stress at any moisture content level. According to Vasilenko et al. (2013), the bulk density's dependence on the consolidation stress can be represented in Eq. 10 (Schulze, 2008), where ρ_b is the bulk density at specific consolidation, ρ_0 is the initial value of bulk density and $\sigma_{cons.}$ is consolidation stress in kPa (Vasilenko et al., 2013).

$$\rho_b = \rho_0 + a \ln(\sigma_{cons.}) \qquad \text{Eq. 10}$$

As seen in Figure 5, although the basic profiles remained comparable, the rise rate for wet samples in relation to the applied normal consolidation load was substantially higher compared to partially dried and dried samples. From morphology and size characterisation (Figure 3 and Figure 4), it can be conceived that the clusters of starch granules appear as the major players in defining the bulk behaviour of the samples, which are prone to be deformed. This deformation may occur either at the granule scale, as reported previously by (Fitzpatrick et al., 2004; Sun, 2016; Salehi et al., 2021) or at the cluster scale. In the latter case, it is anticipated that agglomerates and granules will be rearranged in relation to one another. The presence of water molecules mainly promotes the change in the cluster structures. This statement can be supported by the PSD results shown in Figure 4 graphs, where the drying effect was found to be more remarkable in the particle size range of 100-1000 μm, representing the clusters of starch granules. This finding may help to explain why, regardless of the weight of water lost during drying, the bulk density of wet samples is more sensitive to the amount of the applied normal consolidation load than samples that have been partially dried or dried (Figure 5).

3.3 Failure envelopes and Flow properties

The presence of moisture can prevent pulverised cassava grits from flowing by two main mechanisms. First, it can facilitate the formation of liquid bridges and promote capillary forces between grits. Second, it can also alter the mechanical properties of grits, as Salehi et al. (2021) highlighted the fact that neglecting the change in the particle's plasticity due to the absorbed moisture content led to a significant deviation in the prediction of the actual interparticle forces (Salehi et al., 2021). Hence, to study the flow behaviour of pulverised cassava grits during the drying process, it is necessary to understand the moisture content's effect. The failure envelopes, shown in Figure 6, were constructed for wet and dried samples at four different levels of consolidation stresses, according to the procedure described in section 2.3.

Generally, the failure envelopes become smaller as the drying process progresses. This shrinkage indicates that the flowability was promoted by losing water content, i.e., by applying the same loads, the dried samples began to flow sooner than the wet samples. The impact of the preparation approach was noticeable, as can be seen by the difference between the dashed curves for RAS grits and solid curves for RCB grits. At the larger magnitude of the imposed consolidation stress (2.237 and 4.819 kPa), RAS grits displayed more curvature around the origin, resulting in lower resistance to incipient failure states. Under higher normal loads that end up with the steady-state failures, the dried RCB grits with D50 of 456.92 μm showed a better flowability than the dried RAS grits with D50 of 608.57 μm. However, for wet samples, the impact of grit size was different. The wet samples with smaller grits size (RCB with 473.23 μm) showed better flowability only at the lowest consolidation stress level of 0.482 kPa. The wet samples with larger grit sizes (RAS with 536.54 m) tended to exhibit less resistance to incipient failure states when the consolidation stress increased.

Figure 7 shows how the estimated flow properties of cohesion (Figure 7-a) and tensile strength (Figure 7-b) vary with respect to the physical condition of samples determined by the experienced consolidation stress and the moisture content. The water content's effect was dominant, while the impact of the cassava grits size distribution was also clearly visible but with a lower magnitude.

It is worth noting that there is no general agreement on the reliability of the quantities obtained by the back extrapolation of the measured incipient-failure points. However, when it comes to estimating those quantities without actually measuring them, using the Warren-Spring equation can be a practical and conclusive choice, especially for cohesive materials, as demonstrated in (Ashton et al., 1965; García-Triñanes et al., 2019). Using the nonlinear Warren-Spring model resulted in much more accurate flow property values than the values attained by using the linear model of Mohr-Coulomb (Ashton et al., 1965; García-Triñanes et al., 2019).

The increasing trend of cohesion seen in the graphs at higher consolidation stress in Figure 7.a was alleviated as the product's moisture content was reduced, implying an enhanced flowability of the bulk casava grits. The predicted values for cohesion reached 1.8 kPa at the highest level of consolidation (4.819 kPa) for wet samples with RCB grits. After drying, however, the opposite tendency was seen, with RAS grit samples having slightly higher cohesion values. The effect of particle size, as one of the most important physical attributes, on the flowability of cohesive powders has been previously studied (Teunou et al., 1999). In the lower levels of consolidation in Figure 7-a, the effect of cassava grits size is dominant, where RAS samples showed higher cohesion than RCB samples. Nonetheless, grit size was not the dominant cause on wet samples, and RCB grits showed noticeably higher cohesion indicating a poorer flowability. At the 31% wb. of water content, green graphs in Figure 7-a, the effect of grits size on cohesion has changed with respect to the consolidation stress.

In Figure 7-b, the combined effect of the water content and the consolidation stress on the σ_T values was dominant during the drying process. The obtained values for wet samples were nearly three times higher for C and four times higher for σ_T than dry sample values. This range of variation has significant consequences in the handling of these materials.

A possible mechanism to point out here is the decrease in cohesion during drying as the reduction in the starch granule's surface roughness due to the water evaporation, which reduces the magnitude of interparticle forces. Tensile strength is a magnitude based on the influence of interparticle adhesive forces on the strength of the bulk solid against pure tension loads. Tensile strength is probably linked to bulk density because these forces' magnitude depends on the spacing between the packing particles (García-Triñanes et al., 2019).

According to the results presented in Figure 4, the wet RCB samples showed a significantly higher surface area compared to RAS samples, 70 cm^2/g versus 51 cm^2/g, respectively. Furthermore, the value of D10 accounted for 227.4 μm and 323.6 μm, respectively, for RCB and RAS grits. The contact surface area of cassava grits rises as their size decreases, resulting in increased van der Waals attraction forces between the particles. The readily available water molecules in the finer clusters of RCB grits may cause the augmentation of interparticle interactions. Subsequently, a significant surge is observed in cohesion and tensile strength, especially at the highest consolidation level (4.819 kPa). In support of these findings, other researchers have reported similar behaviour when quantifying flowability indexes (Sun, 2016; Juarez-Enriquez et al., 2019).

3.4 Flowability classification

It is common practice to classify the flowability state into specific groups for bulk solids under a particular consolidation load. Therefore, further evaluations were conducted to reproduce the classic Jenike flowability classification. According to Jenike the flowability can be explained by considering the ratio of σ_c/σ_1, known as flow function (1/*ffc*). This ratio can represent the shape of the failure envelopes in Figure 6, while σ_1 shows the length of the envelope and σ_c can reflect the steepness of the left-hand side of the envelopes. Figure 8-a portrays the flow function values obtained at a different level of consolidation stress, while Figure 8.b shows the ratio considering the relative difference between internal friction angles. $\varphi_e - \varphi_{sf}$ is representing the transition phase between incipient failure and steady-state failure states. Therefore, the shape of the envelopes can also be represented by the geometrical feature of $\Delta\varphi_{e-sf} = \frac{\varphi_e-\varphi_{sf}}{\varphi_{sf}} \times 100$, as depicted in Figure 8-b.

Results imply that the stress history influences both steady-state (right-hand tail of failure envelopes in Figure 6) and the incipient (left-hand tail of failure envelopes in Figure 6) failure points. However, the influence of the consolidation history is eliminated in determining the flow function values. While the same conclusion can be made for $\Delta\varphi_{e-sf}$ of dried samples, the effect of the previous consolidation load was significant in the wet samples, shown as blue markers in Figure 8-b.

Five well-known groups of free-flowing (σ_c/σ_1 < 0.1), easy-flowing (0.1 < σ_c/σ_1< 0.25), cohesive (0.25 < σ_c/σ_1< 0.5), very cohesive (0.5 < σ_c/σ_1< 1) and non-flowing (σ_c/σ_1> 1) were depicted as a colour pallet in Figure 8-a, where lighter colours represent a better flowability. Figure 8-a shows that the wet samples are very cohesive bulk solid, resulting in poor flowability, independent of their consolidation history. Partially dried samples with 31% wb. of water content are placed in the cohesive region. Further drying made the samples with RCB grits completely free-flowing, while the samples with RAS grits were located in a marginal place between easy-flowing and free-flowing. In Figure 8-a, neither the preparation methods used nor the consolidation history is related to the flow function as average values of σ_c/σ_1 at a given moisture content (P<0.05).

It is expected to see that $\Delta\varphi_{e-sf}$ is relatively small for easy-flowing bulk solids (Schulze, 2008). The smaller ratio reflects the linear tendency in constructing the incipient yield locus in Figure 2. That is to say; a steeper transition will be experienced from incipient failure into steady-state failure, which comes with a smaller ratio of $\Delta\varphi_{e-sf}$. This situation can be seen in the lowest range of applied consolidation stress which caused a bulk density range of 450-550 kg/m^3 for the dried samples, whether prepared using RCB or RAS. For the samples with higher bulk density, a slightly smaller $\Delta\varphi_{e-sf}$ would be expected. Overall, $\Delta\varphi_{e-sf}$was much more moisture-dependent rather than being consolidation-dependent.

4 Conclusions

This study provides relevant information on the physical and flow properties of pulverised cassava grits dried from 46% to 14% wb., replicating the materials typically used in small-scale food processing centres in Africa. The morphology of grits was found as irregularly shaped clusters generated by truncated-oval starch granules. At magnifications lower than 30, the effect of the used preparation procedure can be seen. Using rotating abrasive surfaces caused coarser wet grits with D50 of 608.57 µm compared to 456.92 µm for the grits obtained by rotary cutting blades. The effect of moisture content was studied on the bulk density variation to the consolidation stress using a well-known logarithmic equation. There was no significant difference in bulk density due to the preparation techniques. The constructed failure envelopes shrunk as the drying process progressed, showing the decreasing resistance against the plastic flow of bulk cassava grits. Cohesion and tensile strength increased with consolidation stress, specifically at higher moisture content levels. On the contrary, the internal friction angles were a function of the moisture content rather than their consolidation history. The relative difference between effective and steady-state angles of internal friction showed a tendency to be independent of the stress history effect, in particular at lower levels of water content. Therefore, the proposed φ ratio can be applied to rank the flowability of the samples, compared to the classic classification based on flow function values, i.e., wet samples placed in a very cohesive zone, partially dried samples placed in a cohesive zone, and dried samples lied on the limits of the free-flowing zone.

Acknowledgement

The research work was funded by the Food and Nutrition Security Initiative (FaNSI) program, Natural Resources Institute, University of Greenwich, part of Research England' Expanding Excellence in England' funding.

References

Airlangga, B., Puspasari, F., Trisanti, P. N., Juwari, & Sumarno. (2020). Structural Properties Change of Cassava Starch Granule Induced by High Shear Mixer. Starch - Stärke, 72(11–12), 2000004. https://doi.org/10.1002/star.202000004

Amagliani, L., O'Regan, J., Kelly, A. L., & O'Mahony, J. A. (2016). Physical and flow properties of rice protein powders. Journal of Food Engineering, 190, 1–9. https://doi.org/10.1016/J.JFOODENG.2016.05.022

Ashton, M. D., Cheng, D. C.-H., Farley, R., & Valentin, F. H. H. (1965). Some investigations into the strength and flow properties of powders. Rheologica Acta, 4(3), 206–218. https://doi.org/10.1007/BF01969257

Balagopalan, C. (2002). Cassava sutilisation in food, feed and industry. In Cassava: Biology, Production and sUtilisation (pp. 301–318). Eds.; CABI: Wallingford, UK.

Beeching, J. (2001). Identifying Target Points for the Control of Post-Harvest Physiological Deterioration in Cassava. (pp. 4–6). University of Bath, UK.

Berry, R. J., & Bradley, M. S. A. (2007). Investigation of the effect of test procedure factors on the failure loci and derived failure functions obtained from annular shear cells. Powder Technology, 174(1–2), 60–63. https://doi.org/10.1016/J.POWTEC.2006.10.023

Berry, R., Bradley, M., & McGregor, R. (2015). Brookfield powder flow tester – Results of round robin tests with CRM-116 limestone powder. Proceedings of the Institution of Mechanical Engineers, Part E: Journal of Process Mechanical Engineering, 229(3), 215–230. https://doi.org/10.1177/0954408914525387

Dudu, O. E., Li, L., Oyedeji, A. B., Oyeyinka, S. A., & Ma, Y. (2019). Structural and functional characteristics of optimised dry-heat-moisture treated cassava flour and starch. International Journal of Biological Macromolecules, 133, 1219–1227. https://doi.org/10.1016/j.ijbiomac.2019.04.202

Fadeyibi, A., Osunde, Z. D., Agidi, G., & Evans, E. C. (2014). Flow and strength properties of cassava and yam starch–glycerol composites essential in the design of handling equipment for granular solids. Journal of Food Engineering, 129, 38–46. https://doi.org/10.1016/J.JFOODENG.2014.01.006

FAO. (2021). Food and Agriculture Organization of the United Nations, FAO statistical database. www.fao.org. (Accessed 2021, September 14).

Fitzpatrick, J. J., Barringer, S. A., & Iqbal, T. (2004). Flow property measurement of food powders and sensitivity of Jenike's hopper design methodology to the measured values. Journal of Food Engineering, 61(3), 399–405. https://doi.org/10.1016/S0260-8774(03)00147-X

García-Triñanes, P., Luding, S., & Shi, H. (2019). Tensile strength of cohesive powders. Advanced Powder Technology, 30(12), 2868–2880. https://doi.org/10.1016/J.APT.2019.08.017

Han, H., Hou, J., Yang, N., Zhang, Y., Chen, H., Zhang, Z., Shen, Y., Huang, S., & Guo, S. (2019). Insight on the changes of cassava and potato starch granules during gelatinisation. International Journal of Biological Macromolecules, 126, 37–43. https://doi.org/10.1016/J.IJBIOMAC.2018.12.201

Hirota, M., Takenaka, K., Iimura, K., & Suzuki, M. (2007). Proposal of an approximation equation for the yield locus to evaluate powder properties. Advanced Powder Technology, 18(3), 287–302. https://doi.org/10.1163/156855207780860200

Hunter, J. D. (2007). Matplotlib: A 2D Graphics Environment. Computing in Science & Engineering, 9(3), 90–95. https://doi.org/10.1109/MCSE.2007.55

ISO-3310. (2016). ISO-3310-1: Test sieves, technical requirements and testing. International Organization for Standardization.

Lanzerstorfer, C. (2020). Apparent density of compressible food powders under storage conditions. Journal of Food Engineering, 276, 109897. https://doi.org/10.1016/j.jfoodeng.2019.109897

Landillon, V., Cassan, D., Morel, M. H., & Cuq, B. (2008). Flowability, cohesive, and granulation properties of wheat powders. Journal of Food Engineering, 86(2), 178–193. https://doi.org/10.1016/J.JFOODENG.2007.09.022

Juarez-Enriquez, E., Olivas, G. I., Zamudio-Flores, P. B., Ortega-Rivas, E., Perez-Vega, S., & Sepulveda, D. R. (2017). Effect of water content on the flowability of hygroscopic powders. Journal of Food Engineering, 205, 12–17. https://doi.org/10.1016/J.JFOODENG.2017.02.024

Juarez-Enriquez, E., Olivas, G. I., Ortega-Rivas, E., Zamudio-Flores, P. B., Perez-Vega, S., & Sepulveda, D. R. (2019). Water activity, not moisture content, explains the influence of water on powder flowability. LWT, 100, 35–39. https://doi.org/10.1016/J.LWT.2018.10.043

Jung, H., Lee, Y., & Yoon, W. (2018). Effect of Moisture Content on the Grinding Process and Powder Properties in Food: A Review. Processes, 6(6), 69. https://doi.org/10.3390/pr6060069

Plucknett, D. L., Phillips, T. P., & Kagbo, R. B. (2000). A Global Development Strategy for Cassava: Transforming a Traditional Tropical Root Crop Spurring Rural Industrial Development and Raising Incomes for the Rural Poor. In Global Cassava Strategy.

Precoppe, M., Komlaga, G.A., Chapuis, A., Müller, J. (2020). Comparative Study between Current Practices on Cassava Drying by Small-Size Enterprises in Africa. Applied Sciences, 10(21):7863. https://doi.org/10.3390/app10217863

Romuli, S., Abass, A., & Müller, J. (2017). Physical Properties of Cassava Grits before and after Pneumatic Drying. Journal of Food Process Engineering, 40(2). https://doi.org/10.1111/jfpe.12397

Salehi, H., Karde, V., Hajmohammadi, H., Dissanayake, S., Larsson, S. H., Heng, J. Y. Y., & Bradley, M. (2021). Understanding flow properties of mannitol powder at a range of temperature and humidity. International Journal of Pharmaceutics, 596, 120244. https://doi.org/10.1016/J.IJPHARM.2021.120244

Schulze, D. (2008). Powders and Bulk Solids. Springer Berlin Heidelberg. https://doi.org/10.1007/978-3-540-73768-1

Sun, C. C. (2016). Quantifying effects of moisture content on flow properties of microcrystalline cellulose using a ring shear tester. Powder Technology, 289, 104–108. https://doi.org/10.1016/J.POWTEC.2015.11.044

Opaliński, I., Chutkowski, M., & Hassanpour, A. (2016). Rheology of moist food powders as affected by moisture content. Powder Technology, 294, 315–322. https://doi.org/10.1016/J.POWTEC.2016.02.049

Opaliński, I., Chutkowski, M., & Stasiak, M. (2012). Characterising moist food-powder flowability using a Jenike shear-tester. Journal of Food Engineering, 108(1), 51–58. https://doi.org/10.1016/J.JFOODENG.2011.07.031

Teunou, E., & Fitzpatrick, J. J. (1999). Effect of relative humidity and temperature on food powder flowability. Journal of Food Engineering, 42(2), 109–116. https://doi.org/10.1016/S0260-8774(99)00087-4

Teunou, E., & Fitzpatrick, J. J. (2000). Effect of storage time and consolidation on food powder flowability. Journal of Food Engineering, 43(2), 97–101. https://doi.org/10.1016/S0260-8774(99)00137-5

Teunou, E., Fitzpatrick, J. J., & Synnott, E. C. (1999). Characterisation of food powder flowability. Journal of Food Engineering, 39(1), 31–37. https://doi.org/10.1016/S0260-8774(98)00140-X

Vasilenko, A., Koynov, S., Glasser, B. J., & Muzzio, F. J. (2013). Role of consolidation state in the measurement of bulk density and cohesion. Powder Technology, 239, 366–373. https://doi.org/10.1016/J.POWTEC.2013.02.011

Virtanen, P., Gommers, R., Oliphant, T. E., Haberland, M., Reddy, T., Cournapeau, D., Burovski, E., Peterson, P., Weckesser, W., Bright, J., van der Walt, S. J., Brett, M., Wilson, J., Millman, K. J., Mayorov, N., Nelson, A. R. J., Jones, E., Kern, R., Larson, E., … Vázquez-Baeza, Y. (2020). SciPy 1.0: fundamental algorithms for scientific computing in Python. Nature Methods, 17(3), 261–272. https://doi.org/10.1038/s41592-019-0686-2

Westby, A. (2002). Ch.14 Cassava utilisation, storage and small-scale processing. In Hillocks, R. J., Thresh, J. M. CABI. Cassava: biology, production and utilisation. https://doi.org/10.1079/9780851995243.0281

Zhang, L., Zhao, Y., Hu, W., Qian, J. Y., Ding, X. L., Guan, C. R., Lu, Y. Q., & Cao, Y. (2018). Multi-scale structures of cassava and potato starch fractions varying in granule size. Carbohydrate Polymers, 200, 400–407. https://doi.org/10.1016/J.CARBPOL.2018.08.022

Table & Figures

Table 1: Summary of the consolidation normal stresses and over-consolidated failure stresses applied to the cassava samples.

		Yield Locus number			
		1	2	3	4
1	Consolidation normal stress (kPa)	0.482	1.038	2.237	4.819
2	1st over-consolidation failure stress (kPa)	0.096	0.208	0.447	0.964
3	2nd over-consolidation failure stress (kPa)	0.193	0.415	0.895	1.928
4	3rd over-consolidation failure stress (kPa)	0.289	0.623	1.342	2.891
5	4th over-consolidation failure stress (kPa)	0.386	0.831	1.789	3.855
6	Consolidation normal stress (kPa) *	0.482	1.038	2.237	4.819

* Measurement points for checking consistency according to (R. Berry et al., 2015)

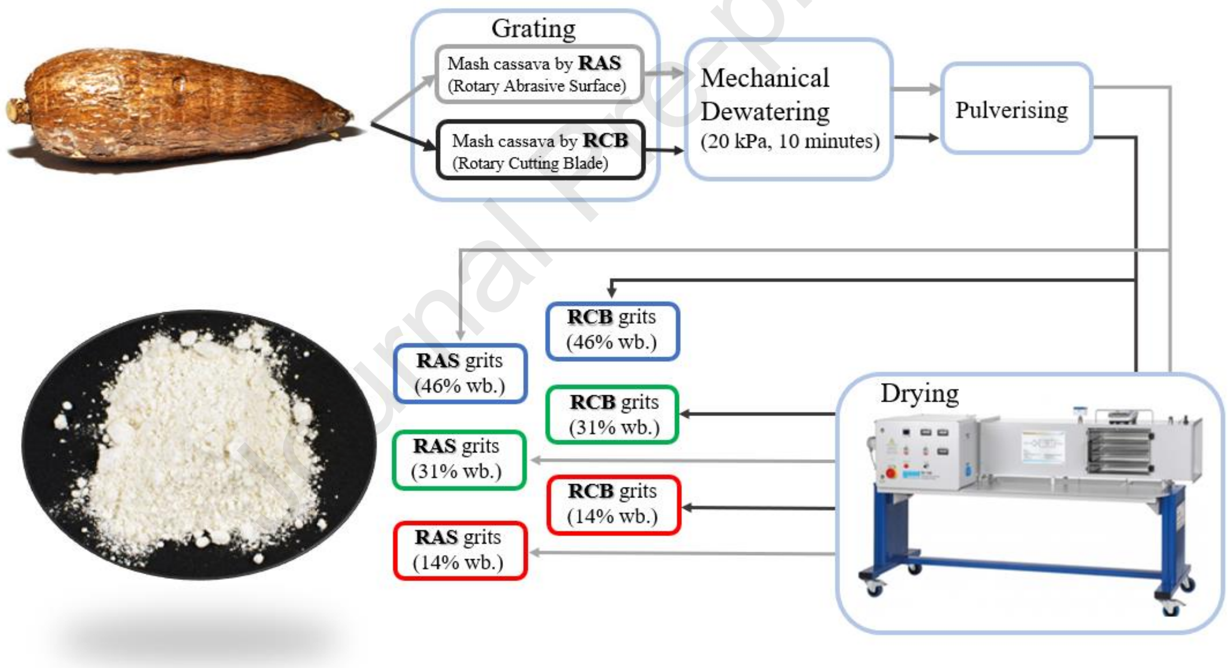

Figure 1: Subsequential stages of preparing different samples of pulverised cassava grits, grated with either RAS or RCB, at three levels of moisture contents using a laboratory convection drying equipment of GUNT CE130, Germany.

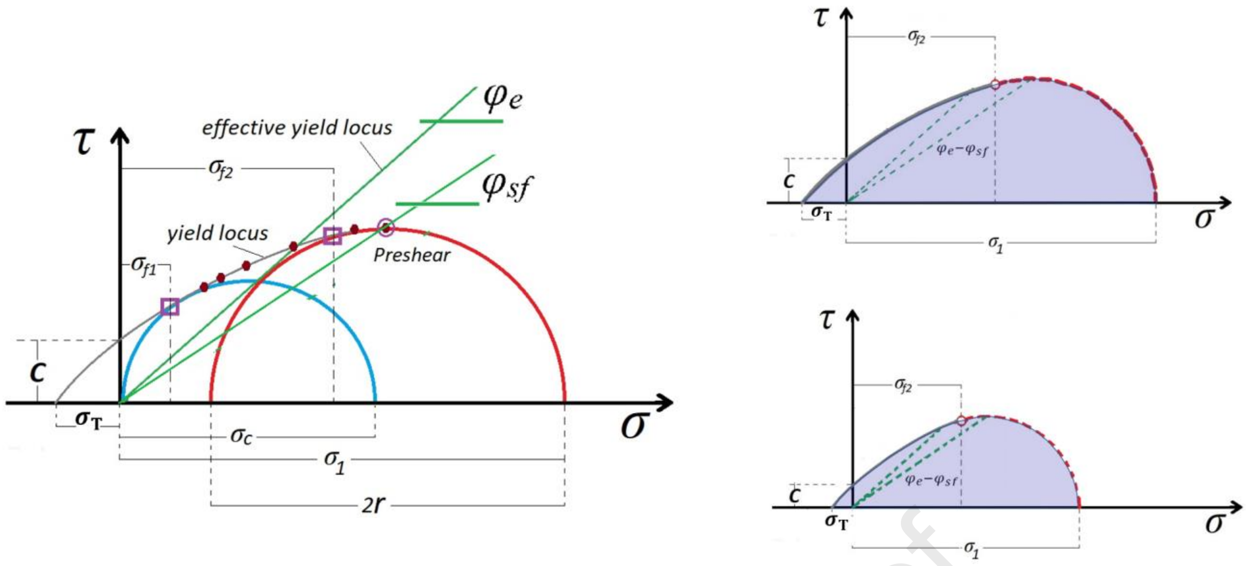

a) Flow properties

b) Failure envelopes

Figure 2: Schematic of the failure envelopes in the stress plane. a) shear-to-failure points (●) and their yield locus at a certain level of consolidation stress illustrating the flow properties of cohesion (C), tensile strength (σ_T), unconfines yield strength (σ_c), major principal consolidation normal stress (σ_1), normal stress at the failure plane of unconfined uniaxial compression test (σ_{f1}), and normal stress at the endpoint of yield locus (σ_{f2}). b) Two examples of failure envelopes in the stress plane.

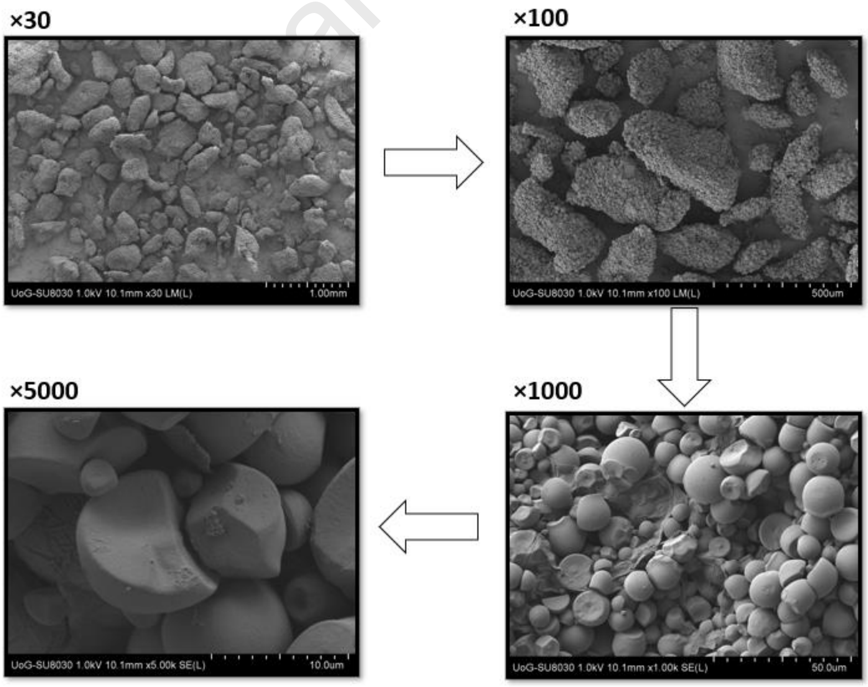

Figure 3: Morphology of RCB cassava grits captured by scanning electron microscopy imaging at four different magnification levels of ×30, ×100, ×1000, ×5000 represented clockwise.

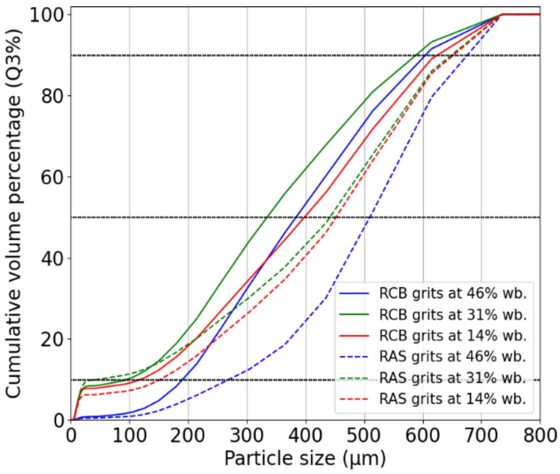

a) Laser Diffraction Analysis

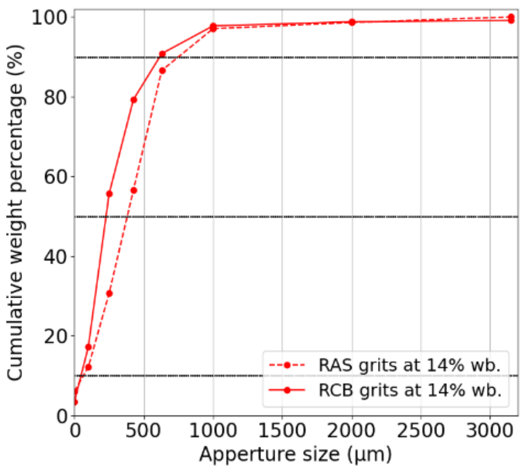

b) Sieving results

	Volume based						Weight based	
	46 % wb.		31 % wb.		14 % wb.		14 % wb.	
	RCB	RAS	RCB	RAS	RCB	RAS	RCB	RAS
D10 (µm)	227.37 ± 0.77	323.55 ± 6.21	113.16 ± 0.71	53.94 ± 4.52	141.10 ± 25.21	183.64 ± 19.93	55 ± 1.23	85 ± 2.42
D50 (µm)	456.92 ± 4.29	608.57 ± 4.67	399.90 ± 10.63	523.45 ± 6.75	473.23 ± 10.63	536.54 ± 14.63	225 ± 3.71	385 ± 4.96
D90 (µm)	724.25 ± 2.35	806.43 ± 2.01	703.56 ± 8.98	774.98 ± 3.16	747.41 ± 8.97	755.63 ± 2.63	605 ± 12.34	685 ± 8.15
Span	1.807	0.793	1.476	1.377	1.281	1.066	2.44	1.558
SSA (cm^2/g)	69.84 ± 0.33	50.94 ± 0.45	197.69 ±33.4	203.29 ± 10.67	197.01± 33.4	165.63± 10.27		

c) Size characterisations

Figure 4: Particle size characterisations of the samples of cassava grits prepared by RCB, solid curves, and RAS, dashed curves, at different levels of water content; blue colour stands for wet samples of 46% wb, green colour stands for partially dried samples of 31% wb., and red colour stands for dried samples of 14% wb, obtained first by a) Volume based method of laser diffraction analysis and second by b) Weight based method of sieving for dried samples.

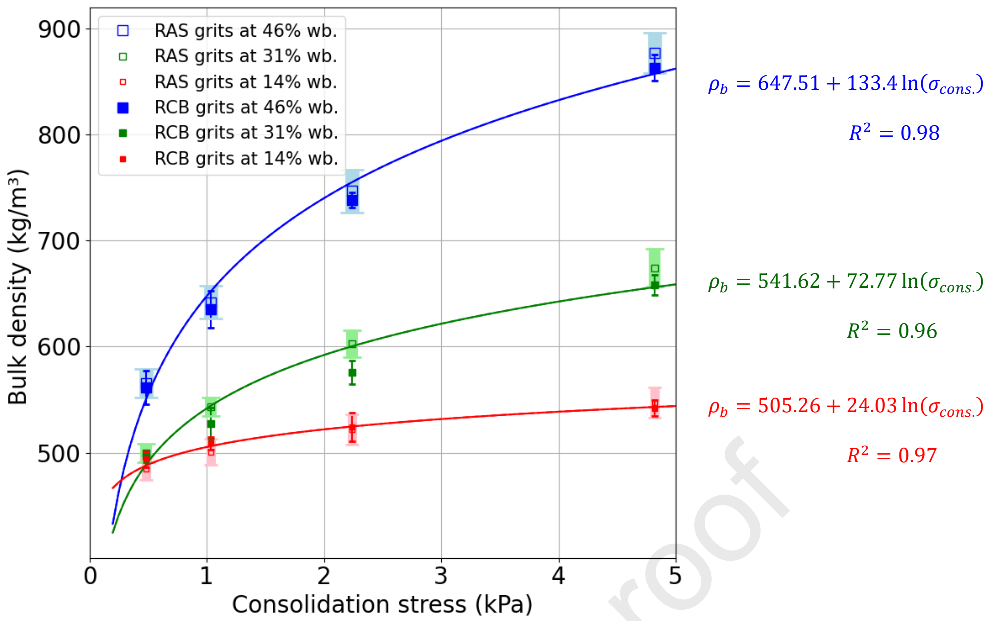

Figure 5: Bulk density of the samples of cassava grits prepared by RCB, ■ with line errorbar, and RAS, □ with strip errorbar, at different levels of water content; blue colour stands for wet samples of 46% wb, green colour stands for partially dried samples of 31% wb., and red colour stands for dried samples of 14% wb. along with their regressed logarithmic equation (Eq.10).

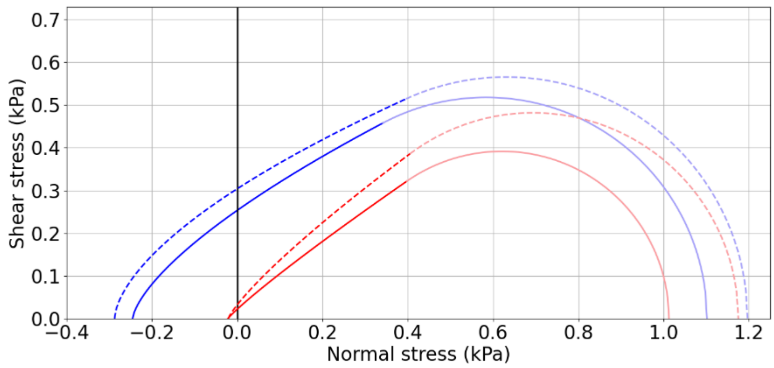

a) Consolidation stress of 0.482 kPa

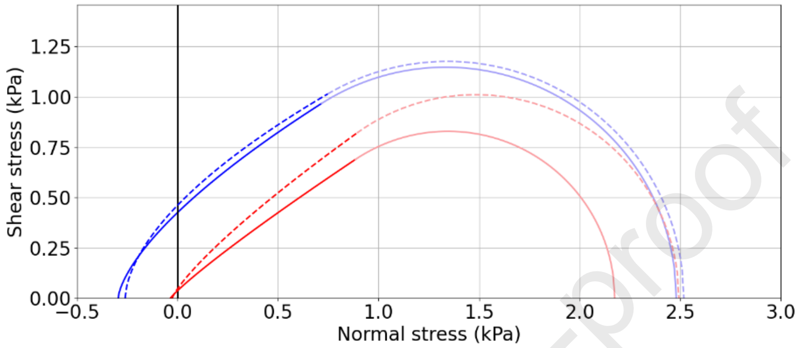

b) Consolidation stress of 1.038 kPa

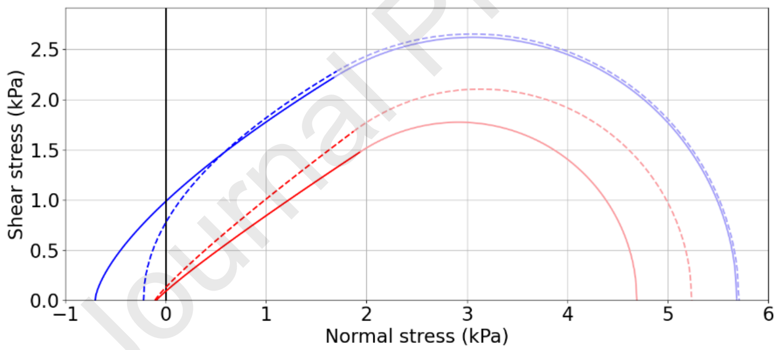

c) Consolidation stress of 2.237 kPa

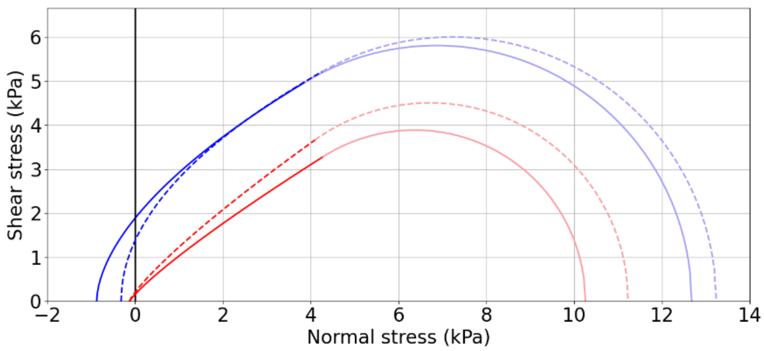

d) Consolidation stress of 4.819 kPa

Figure 6: Failure envelops of the cassava samples; blue colour stands for 46% wb and red colour stands for 14% wb of moisture content; solid lines for RAS grits and dashed line for RCB grits; dark colour for incipient failure and light colour for steady-state failure

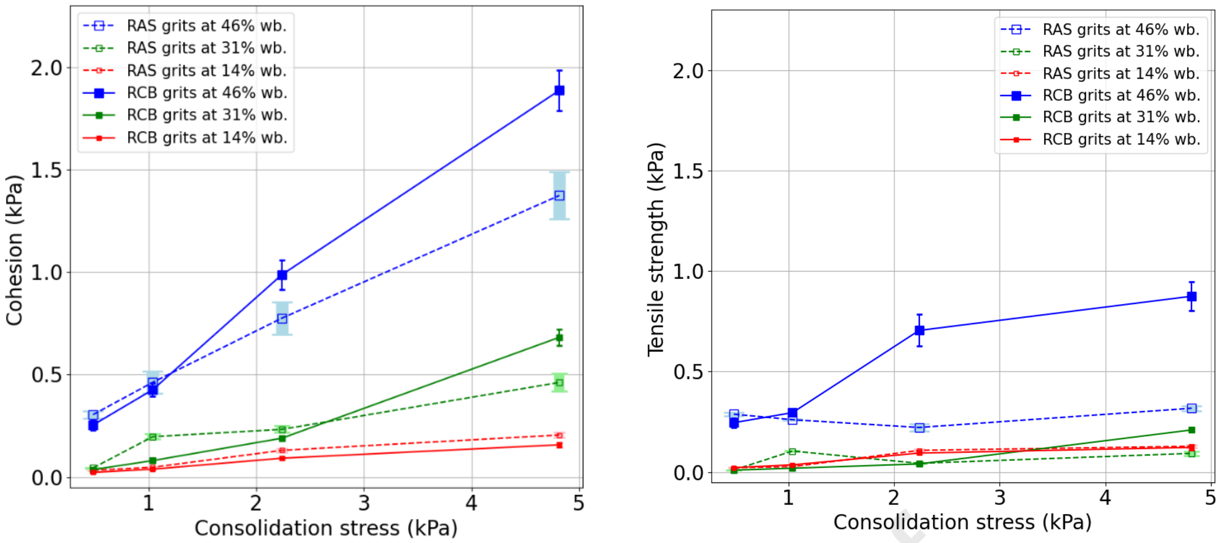

a) Cohesion b) Tensile strength

Figure 7: Cohesion and tensile strength with respect to the applied consolidation stresses; for the samples prepared by RCB, ■ with line errorbar, and RAS, □ with strip errorbar, at different moisture content levels; blue colour stands for 46% wb, green colour stands for 31% wb., and red colour stands for 14% wb.

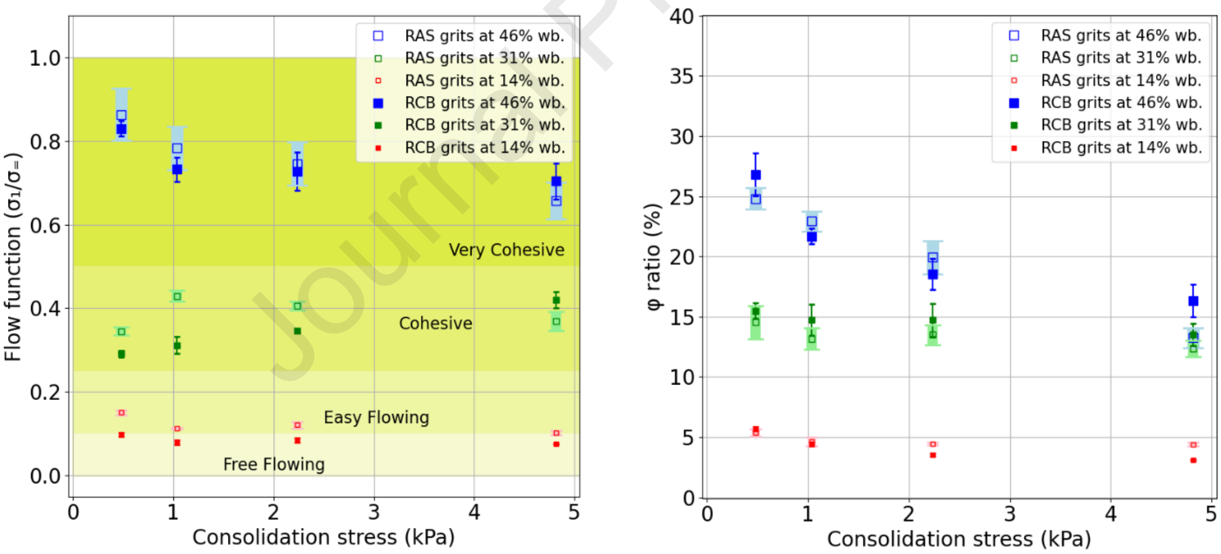

a) Flow function (σ_c/σ_1) b) $\Delta\varphi_{e-sf} = \frac{\varphi_e - \varphi_{sf}}{\varphi_{sf}} \times 100$

Figure 8: Flowability of the pulverised cassava grits under different consolidation stress, characterised by the Jenike flow function σ_c/σ_1 (a) and the relative difference between internal friction angles $\Delta\varphi_{e-sf}$ (b) for the samples prepared by RCB, ■ with line errorbar, and RAS, □ with strip errorbar, at different moisture content levels; blue colour stands for 46% wb, green colour stands for 31% wb., and red colour stands for 14% wb.

Highlights

1. Samples were mashed using rotary abrasive surface and rotary cutting blade methods
2. Pulverised cassava grits were dried from 46% to 14% wb. using a convection dryer
3. Morphology and size features of grits were studied using sieving, SEM, and LDA
4. Shear testing conducted using PFT over 0.418 to 4.892 kPa range of consolidation
5. Water content and grits sizes determines the flowability during the drying process

Declaration of Competing Interest

The authors declare that they have no known competing financial interests or personal relationships that could have appeared to influence the work reported in this paper.